Analyst

Mapping chemotherapeutic drug distribution in cancer cell spheroids using 2D-TOF-SIMS and LESA-TIMS-MS

Journal:	*Analyst*
Manuscript ID	AN-ART-11-2019-002245.R3
Article Type:	Paper
Date Submitted by the Author:	07-Aug-2020
Complete List of Authors:	Cintron Diaz , Yarixa ; Florida International University, Chemistry and Biochemistry Acanda de la Rocha, Arlet Maria; Florida International University, Chemistry and Biochemistry Castellanos, Anthony; Florida International University, Chemistry and Biochemistry Chambers, Jeremy; Florida International University, Chemistry and Biochemistry Fernandez-Lima, Francisco; Florida International University, Chemistry and Biochemistry

Journal Name

ARTICLE

Mapping chemotherapeutic drug distribution in cancer cell spheroids using 2D-TOF-SIMS and LESA-TIMS-MS

Received 00th January 20xx,
Accepted 00th January 20xx

DOI: 10.1039/x0xx00000x

www.rsc.org/

Yarixa L. Cintron-Diaz[a], Arlet M. Acanda de la Rocha[b], Anthony Castellanos[a], Jeremy Chambers[b] and Francisco Fernandez-Lima[a].

Three-dimensional (3D) cancer cell cultures grown in the form of spheroids are effective models for the study of *in-vivo-like* processes simulating cancer tumor pharmacological dynamics and morphology. In this study, we show the advantages of Time -of -Flight Secondary Ion Mass Spectrometry (TOF -SIMS) combined with *in-situ* Liquid Extraction Surface Analysis coupled to trapped Ion Mobility Spectrometry Mass Spectrometry (LESA-TIMS-TOF MS) for high spatial resolution mapping and quantitation of ABT-737, a chemotherapeutic drug, at the level of single human colon carcinoma cell spheroids (HCT 116 MCS). 2D-TOF-SIMS studies of consecutive sections (~16 µm thick slices) showed that ABT-737 is homogenously distributed in the outer layers of the HCT 116 MCS. Complementary *in situ* LESA-TIMS-TOF MS/MS measurements confirmed the presence of the ABT-737 drug in the MCS slides by the observation of the molecular ion $[M+H]^+$ m/z and mobility, and charateristic fragmentation pattern. The LESA-TIMS-TOF MS allowed a quantitative assessment of the ABT-737 drug of the control MCS slice spiked with ABT-737 standard over the 0.4 – 4.1 ng range and MCS treated starting at 10µM for 24h. These experiments showcase an effective protocol for unambigous characterization and 3D mapping of chemotherapeutic drug distribution at single MCS level.

Introduction

Three-dimensional multicellular spheroids (MCSs) are emerging as an alternative model to study the physiology of cancer tumors and evaluate drug distribution within a tumor[1]. These 3D tumor models permits the analysis of *in-vivo-like* processes and cell conditions, including differences in cell types within each MCS[2]. When compared to the use of animal models to follow tumor development, MCS present several advantages in reproducibility, rate of growth and cost effectiveness[3].

Mass spectrometry (MS) techniques have been used for the study of various cancers[4, 5], ranging from cancer cell proteomics to clinical applications[6]. MS has proven to be a powerful tool to investigate the molecular content from biological samples and to map at the molecular level their complex spatial distributions[7]. For example, in the case of MCS, MS has been successfully employed to identify extracellular compounds[8]. Mass spectrometry imaging (MSI) has provided information on the protein content within MCS[9]. Chemotherapeutic agents and their metabolites (e.g. Irinotecan and their metabolites) have been characterized in MCS with high spatial resolution MS[10].

[a] *Department of Chemistry and Biochemistry, Florida International University, 11200 SW 8th St., AHC4-233, Miami, FL 33199, United States.*
[b] *Department of Environmental Health Sciences, Florida International University, 11200 SW 8th St., AHC4-233, Miami, FL 33199, United States.*

Recent advancements in ion sources for Secondary Ion Mass Spectrometry (SIMS) has extended their use in biological applications with high spatial resolution (submicrometric)[11]. In a recent work, we showcase the potential of SIMS to follow the drug delivery of ABT-737 at the single cell level using 3D-TOF SIMS[12]. In addition, SIMS has been successfully applied to differentiate cancerous and non-cancerous tissues based on lipid profiles, and it has been suggested as diagnostic tools for screening purposes[13].

While most of the MSI probes require special sample preparation, Liquid Extraction Surface Analysis (LESA) is rapidly emerging as an ambient pressure solution for fast screening and characterization of biological samples that can be easily coupled to traditional MS workflows (e.g., lipid[14, 15] and protein[16-18] profiling). When complemented with other separation techniques (e.g., Liquid chromatography, LC[19], and/or ion mobility spectrometry, IMS[20-22]), LESA can provide extensive characterization with minimum sample preparation[14]. Previous reports have demonstrated how LESA can serve as a profiling tool for drug and metabolite distribution (e.g. terfenadine and chloroquine) in whole-body tissue sections[23, 24]. It has also been proved how LESA can be used for lipidomic profiling of various cancer cell lines[15].

In this study, we showcase the potential of MSI-TOF-SIMS for the identification, localization, and distribution of ABT-737 drug in a HCT 116 cell spheroid model. ABT-737 is a Bcl-2 small-molecule inhibitor which has been proved to be beneficial in preclinical and clinical cancer treatment[25]. ABT-737 is a BH3 mimetic drug that, by binding and inhibiting Bcl-2

proteins, promotes pro-apoptotic proteins that trigger dell death[26]. The use of TOF-SIMS allows for high spatial resolution analysis. Complementary *in situ* LESA-IMS-MS measurements will increase the confidence and quantify the levels of ABT-737 per MCS as a function of the drug concentration in the cell media. IMS has shown many advantages for trace detection of small molecules (e.g., explosives[27], illicit drugs[28], petroleum[29], and natural products[30] among others). In particular, one of the IMS variants, trapped IMS (TIMS[31-33]) has shown several advantages due to higher mobility resolution[34], ease of coupling to MS and high sensitivity in a wide range of analytical applications (e.g., small molecules[35-38], proteomics[39, 40], lipidomic[41], and DNA[42, 43] among others). The ABT-737 drug per MCS secondary conformation and quantitation will be performed based on the ABT-737 $[M+H]^+$ mobility and fragmentation pattern in a LESA-TIMS-TOF MS/MS platform.

Experimental

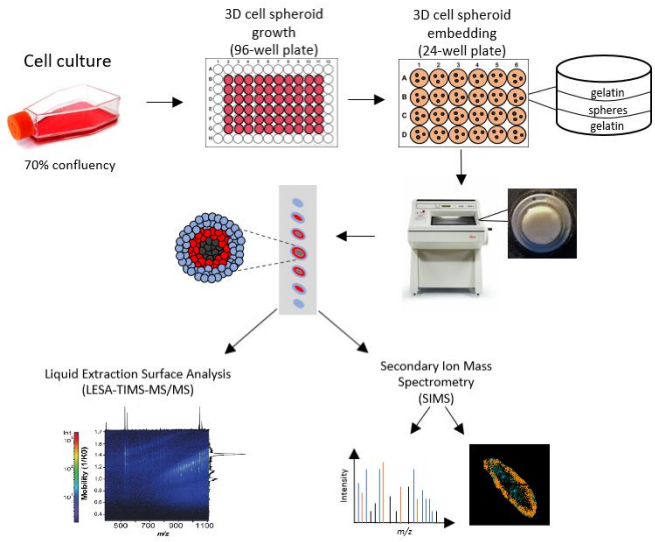

Figure 1. Workflow for MCS characterization using TOF-SIMS for chemical mapping and *in situ* LESA-TIMS-MS/MS for drug delivery secondary confirmation and quantitative analysis.

Cell Culture

Human colon cancer cell line HCT-116 was purchased from American Type Culture Collection (ATCC, Manassas, VA). Cell line was cultured according to the supplier's instructions in McCoy's 5A media (Corning), supplemented with 10% Fetal Bovine Serum (Gibco), 1000 U/mL Penicillin, 100 mg/mL Streptomycin (Gibco), 1% l- glutamax and 5 µg/mL Plasmocin (Invivogen, San Diego, CA). Cells were grown under normal cell culture conditions at 37 °C and under 5% CO_2. Cell passage was performed every four days. HCT-116 cell line was used within three months after resuscitation of frozen aliquots thawed from liquid nitrogen. The provider assured the authentication of these cell lines.

MCS formation

Friedrich et al. protocol was used to generate the spheres in a flat-bottomed 96-well microtiter plates (ThermoFisher)[44]. Briefly, an agarose solution was prepared by dissolving 0.15 g of agarose (Bio-Rad, Hercules, CA) in 10 mL of McCoy's 5a cell culture media and autoclaved for 30 min at 120 °C and 200 kPa. A volume of 50 µL of the agarose solution was added to the inner 60 wells of a 96-well plate. The agarose solidified in around 30 s after being transferred into the well. The plate was covered to allow it to cool down at room temperature and then stored in a 4°C refrigerator.

Cell suspension was prepared by enzymatic dissociation using a 0.25% Trypsin solution (Gibco) and the cells were counted using a hemocytometer. The cell suspension was diluted in McCoy's 5A cell culture media to ~30 cells/µL. Cells were seeded into each of the wells in the agarose-coated cell culture plate at a density of 6000 cells/well in a final volume of 200 µL/well. The cells were incubated under normal cell culture conditions at 37 °C and under 5% CO2, and the culture media was carefully replenished every 3-5 days until spheres reached an average size of 1 mm. The uniform and compact MCSs were used for follow-up studies. MCSs were analyzed in biological triplicates.

Drug Treatment of MCSs

BH3-only mimetic ABT-737 was purchased from Santa Cruz Biotechnology (Dallas, TX, USA). The stock solution of ABT-737 was prepared in dimethyl sulfoxide (DMSO; Sigma-Aldrich, St. Louis, MO, USA) and further diluted into McCoy's 5A cell culture media as needed. We evaluated the efficacy after 72 hours of MCS exposure to ABT-737 over a 0 -100µM range. The relative amount of cell death in the population of cells outside of the necrotic core of the MCS was determined using Calcein AM staining combined with propidium iodide, as previously reported[45, 46]. An IC_{50} of 28 ± 12 µM was detected for ABT-737 cells in HCT-116 MCS at 72 hours. The reported IC_{50} cell viability value of ABT-737 in HCT-116 cells is 17.5 µM[47]. Moreover, during clinical treatment, the ABT-737 plasma concentration levels 5.4 – 7.7 µM[48]. Since the IC_{50}value measured for MCS is likely supraphysiological, we treated the MCS starting with a lower range to address clinically-relevant levels[47,48]. That is,MCSs were treated for 24 h with varying drug concentrations: control, 1 µM, 5 µM, 10 µM, 15 µM, 25 µM, 50 µM, and 100 µM. The treatment time was chosen to assure drug uptake without significant cell death. Untreated MCSs were used for control purposes.

MCSs embedding and cryosectioning

A 24 well plate was prepared by adding 100 uL of warm gelatin into each well, as proposed by Li and collaborators[9]. Cell spheroids were gently transferred via a serological pipette and placed on top of the already solidified gelatin. A second layer of 100 µL of gelatin was added to cover the spheroids. The 24 well plate was stored in a -80° C freezer before sectioning. The embedded cells were removed from the 24 well plate and sliced to 16 µm thickness using a Leica CM 3050 cryostat (Leica

Biosystems, Nussloch, Germany) and thaw mounted into glass slides. Approximately 20 slices at varying depths per MCS were obtained, but only the top half (~10 slices) of the MCS was sampled.

Liquid Extraction Surface Analysis coupled to Trapped Ion Mobility Spectrometry-Mass Spectrometry (LESA-TIMS-MS/MS)

Glass slides with MCS slices were placed on the LESA universal adaptor plate and the location of extraction was manually identified. Liquid Extraction Surface Analysis (LESA) was performed using a TriVersa Nanomate device (Advion, Ithaca, NY, USA) in micro-junction mode. To perform the extraction, an automated arm was relocated on top of the solvent well and aspirated 5 µL of solvent. The robotic arm relocated on top of the desired spot in the MCS sample and descended to a 1.9 mm dispensation height to place 1.0 µL of solvent and form a liquid micro junction between the surface and the solvent. Solvent droplet stayed in contact with the surface for 10 s, re-aspirated and re-dispensed for another 10 s. After this time, 1.5 µL of solvent was re-aspirated and dispensed into a specific well in a 96 well plate. Each extraction covered the entire MCS section on the slide. A peptide internal standard (Human Angiotensin II, 1046 m/z) was prepared to 1 µM concentration and added to the extraction solvent ethanol, water and formic acid (60:39.9:0.1); the peptide internal standard allowed to correct for variations in the LESA tip extraction and nESI spraying conditions across experiments. A calibration curve was developed using control MCS slides spiked with a 0.5 µL drop of ABT-737 standards in the 0.406-4.066 ng range. The calibration curve points used were 0.406 ng, 0.813 ng, 1.219 ng, 1.626 ng, 2.033 ng, 3.253 ng, and 4.066 ng). Extraction was performed as previously described.

A volume of 5 µL of LESA extract was loaded in a quartz glass pull-tip capillary (O.D.: 1.0mm and I.D.: 0.70mm) and sprayed at 600 – 1000 V into a custom built nESI-TIMS coupled to a Bruker impact q-TOF Mass Spectrometer (Bruker Daltonics, Billerica, MA, USA)[16]. The TOF component was operated at 10 kHz and m/z range from 50 - 2000, using the maXis Impact Q-TOF acquisition program. The TIMS component was operated by Lab View, an in-house software, in synchronization with the TOF controls[17]. Details regarding the TIMS operation and calibration procedure can be found elsewhere[17-20]. The ion mobility is determined by,

$$K_0 = \frac{V_g}{E} = \frac{A}{V_{elution} - V_{out}}$$

where K_0 is the reduced mobility, v_g is the gas flow velocity, $V_{elution}$ is the elution voltage and V_{out} is the base voltage. The constant A was determined using a Tuning Mix (Agilent Technologies, Santa Clara, CA, USA) calibration standard of known reduced mobilities. The separation was carried out using Nitrogen (N_2) at room temperature (T) with a gas flow velocity determined by the difference between the funnel entrance pressure (P1 = 2.6 mbar) and the funnel exit pressure (P2 = 1.1 mbar)

Collision cross section (CCS, Ω) were determined by the Mason-Schamp equation:

$$\Omega = \frac{(18\pi)^{1/2}}{16} \frac{z}{(k_B T)^{1/2}} \left[\frac{1}{m_i} + \frac{1}{m_b}\right]^{1/2} \frac{1}{K_0} \frac{1}{N^*}$$

where z is the ion charge, k_B is the Boltzmann constant, N* is the number density, and m_i and m_b are the masses of the ion and bath gas, respectively[49]. Tandem mass spectrometry (MS/MS) experiments were obtained using collision induced dissociation (CID). The mobility profiles and fragmentation patterns of the ABT-737 doped MCS were compared to those of the ABT-737 standard for validation. Data from the LESA-TIMS-TOF MS/MS was analyzed using DataAnalysis version 5.2 and all IMS values were determined using OriginPro version 8.0.

Secondary Ion Mass Spectrometry (SIMS)

Glass slides containing MCS slices were freeze-dried using a custom-built vacuum drier for 2 h, similar to our previous report[10]. Samples were slowly warmed up to room temperature and transferred into the TOF-SIMS analysis vacuum chamber.

A TOF-SIMS instrument (ION-TOF, Münster, Germany) equipped with a high spatial resolution liquid metal ion gun analytical beam (25 keV, Bi3+) was used for chemical mapping. The instrument was operated in high current bunched (HCBU) spectral mode at a current of 0.215 pA and a total primary ion dose of ~5 × 1012 ion/cm2. Charge accumulation was compensated using a low energy electron flooding gun (21 ev). Secondary ions were detected by a hybrid detector, composed of a micro-channel plate, a scintillator, and a photomultiplier[50], efficiently transmitting low mass ions (m/z < 2000). A mass resolving power of m/Δm ~6,000 at m/z 400 and spatial resolution of 1.2 µm was measured in negative polarity analyses. Secondary ion images were collected with the 2D large area stage raster mode with a field of view of 1.0 mm x 1.0mm, a patch side length of 0.3 mm (total 16 patches) and a pixel density of 256 pixels/mm.

Data from the TOF-SIMS was analysed using SurfaceLab 6 software (ION-TOF, Münster, Germany). An internal calibration was achieved with C^-, CH^-, CH_2^-, C_2^-, C_3^-, C_4H^- and $C_{18}H_{33}O_2^-$. After obtaining a full 2D large area image, regions of interest (ROI) were selected based on the distribution of ABT 737 in the MCSs.

Results and Discussion

The formation and growth of 3D HCT 116 cancer cell spheres is a fast and reliable way of studying cancer tumor models in a relatively cheap and quick manner[51]. The spheres assimilate cancer tumors by having the same structure of a poorly vascularized tumor where the outer cells have access to nutrients and the inner cells become hypoxic, leading to cell death[52]. The growth of MCS was monitored every 2-3 days to have a closer inspection of the growth rate. After 15 days, thspheres had grown to around 1mm (Figure 2.a), which is an

optimal size to exhibit 3D cell-cell and cell-matrix interactions and establish chemical gradients of oxygen, nutrients and catabolites[53].

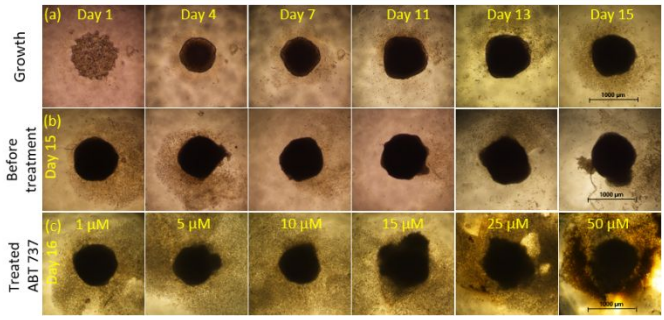

Figure 2. Typical HCT 116 MCS. (a) Optical images (4x) of the same MCS growth as a function of the culture time in a 15-day interval (b) Optical images (4x) of different MCS at day 15 prior to treatment and (c) Optical images (4x) of MCS shown in (b) after 24 hours exposure to ABT-737 at different concentrations.

Our goal was to assess whether clinically-relevant concentrations of ABT-737 could be detected within MCS. MCS were treated with increasing concentrations of ABT-737 which resulted in some cellular detachment from the sphere shape after 24 hours; in particular, at higher concentrations of ABT 737 some spheres lost their shape making it hard to section and transfer for TOF-SIMS analysis. MCS treated with 1 µM, 5 µM, 10 µM, 15 µM, 25 µM and 50 µM of ABT 737 maintained the spherical shape, although cellular detachment was also observed to a lesser extent. In Figure 2 we can observe how each MCS was before (b) and after treatment (c).

The TOF-SIMS analysis under HCBU mode provided high mass resolution and permitted the detection of the ABT-737 molecular ion (i.e., $[M-H]^-$ at 811 *m/z*). The comparison between the TOF-SIMS analysis of control MCS, ABT-737 standard and MCS treated with ABT-737 drug can be found in Supporting Information Figure 1. Closer inspection of SI1 shows that there is no signal at 811 *m/z* for the control MCS samples, whereas there is a predominant signal in the ABT-737 standard and ABT-737 treated MCS samples. This high contrast allowed for the chemical mapping of ABT-737 without major endogenous interferences.

To visualize the distribution of ABT-737 in the MCS, Figure 3 a-b presents optical and TOF-SIMS images of consecutive MCS slices. Across the 16 µm thick slices, there is consistently a high contrast between the 811 *m/z* signal observed from the control MCS (low intensity background) and the ABT-737 treated MCS samples. Endogenous signals at 159 *m/z* (nuclei marker $HP_2O_6^-$) and 255.23 m/z (fatty acid 16:0, $C_{18}H_{33}O_2^-$) allowed for visualization of the MCS on the glass slide. Closer inspection of 811 *m/z* in Figure 3b shows that the 811 m/z signal corresponding to the ABT-737 drug distribution from the ABT-737 treated MCS is clearly defined and restricted to the outer layers of the MCS, while the homogenous distribution of 811 m/z from the control MCS is just a low signal background. A line scan shows the intensity of the 811 *m/z* ion across the sphere and how it is highly intense in the borders and less intense in the center for the case of the ABT-737 treated MCS. A three-dimensional visualization is provided to aid the correlation between the MCS slices and the original 3D MCS (Figure 3b right panel); in the 3D MCS schematic, the ABT-737 signal (gold color) from the outer MCS layers is consistently observed across the slices. While TOF-SIMS analysis of MCS and comparison with between MCS control, ABT-737standard, and ABT-737 treated MCS provided a clear localization and identification of the ABT-737 drug, secondary confirmation was obtained using *in-situ* LESA-TIMS-TOF MS/MS analysis.

Previous reports have shown the existence of multiple components at the level of nominal mass in biological samples[54]. Mobility selected fragmentation patterns were utilized for confirmation of the presence of ABT-737 in the treated MCS samples. One of the remarkable advantages of the LESA-TIMS-TOF MS/MS workflow is the fast screening from biological surfaces at ambient pressure (Figure 4). A typical LESA extraction is performed in less than 1 minute for a single point analysis (~1mm spatial resolution), followed by a short MS analysis, lasting less than 5 minutes per sample, which is a major advantage compared to long LC-MS run times. Different from the TOF-SIMS analysis, the LESA-TIMS-TOF MS was performed in positive ion mode using a nESI source, since better S/N was -

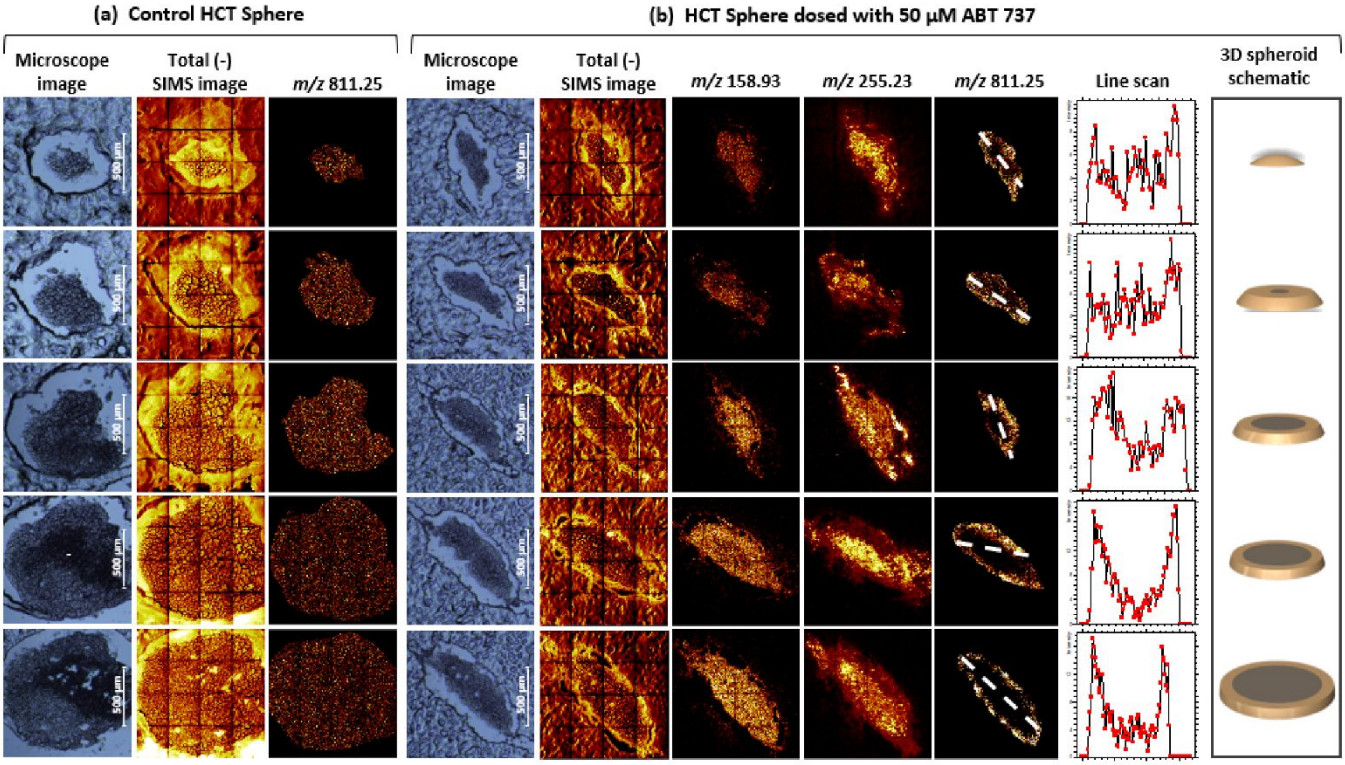

Figure 3. (a) Optical (4x), total SI and m/z 811.25 (ABT-737 $[M-H]^-$) images (left to right) of consecutive control MCS slices. (b) Optical (4x), total SI, endogenous markers (*m/z* 159.93 $HP_2O_6^-$ nuclei marker, *m/z* 255.23 $C_{18}H_{33}O_2^-$,Fatty Acid 16:0$[M-H]^-$), and *m/z* 811.25 (ABT-737 $[M-H]^-$) images (left to right) of consecutive slices from a 50 µM ABT-737 treated MCS. The line scan shows the intensity of ABT-737 across each slice of the spheroid.

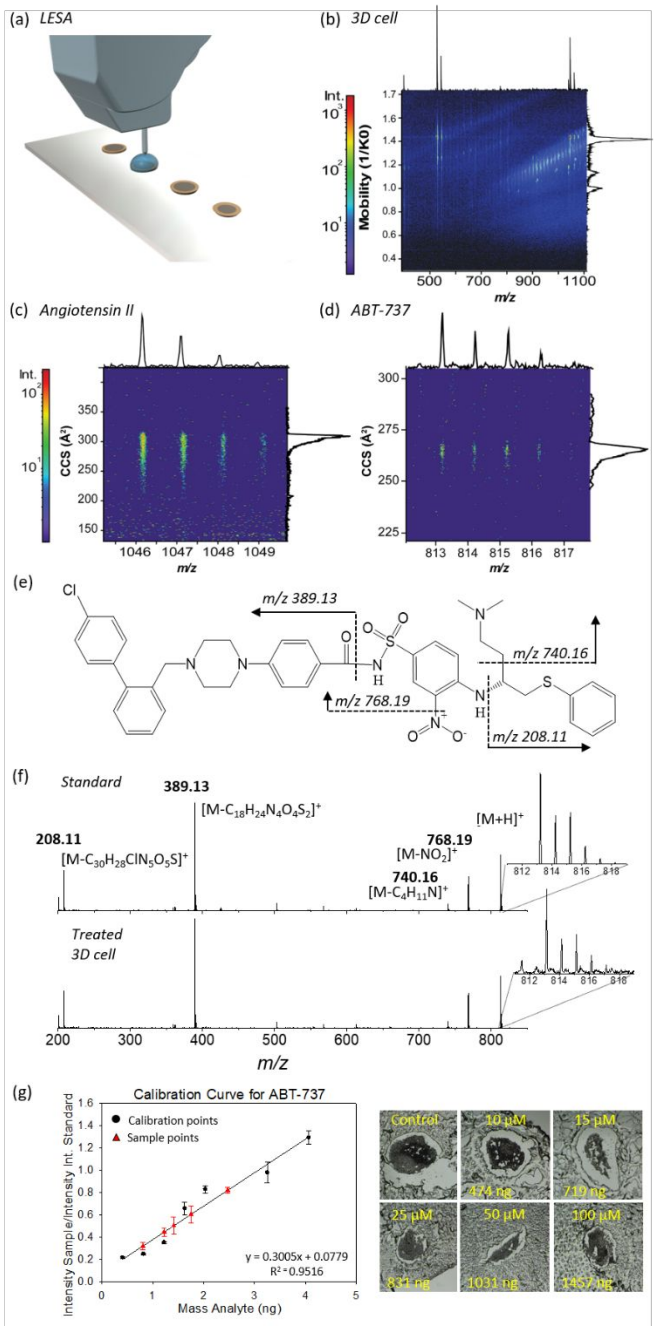

Figure 4. (a) Schematic representation of the LESA extraction. (b) typical 2D-IMS-MS plots of from a 100 µM ABT-737 treated MCS, (c) 2D-IMS-MS blowouts of the Angiotensin II IS and ABT-737 signals. (e) ABT-737 typical fragmentation channels (f) mobility selected MS/MS spectra of the ABT-737 $[M+H]^+$ signal from a standard and from a treated MCS (g) ABT-737 Calibration curve from LESA-TIMS-MS extracted from the MCS slices as a function of the ABT-737 concentration in the culture media. Error bars represent the standard deviation of the measurements (n=3).

observed for the ABT-737 parent ion signal from the complex biological mixture across experiments. The extraction solvent ethanol, water and formic acid (60:39.9:0.1) - was chosen based on the affinity of ABT-737 drug to bind to the hydrophobic grooves of BCl-2 type proteins[55]. The 2D-IMS-MS contour maps allow for a quick identification of the ABT-737 parent ion (813 m/z, $[M+H]^+$) and the Angiotensin II internal standard signal (1046 m/z, $[M+H]^+$) by their *m/z* (~1 ppm mass accuracy) and CCS values in the complex mixture biological extract. The CCS value for ABT-737 $[M+H]^+$ and Angiotensin II $[M+H]^+$are 273 Å^2 and 303 Å^2, respectively. In addition to the accurate mass and mobility of the parent ions, mobility selected MS/MS were used for tertiary confirmation of the ABT 737 signal using the fragment ions $[M-NO_2]^+$, $[M-C_4H_{11}N]^+$, $[M-C_{18}H_{24}N_4O_4S_2]^+$, and $[M-C_{30}H_{28}ClN_5O_5S]^+$.

A calibration curve for ABT-737 using LESA-TIMS-TOF MS was generated from MCS control samples spiked at different concentrations of ABT-737. The extractions were performed in triplicates and the extraction volume covered the entire MCS sections. The amount of drug per slice was determined from the linear regression of the calibration curve (Figure 4g). The calibration curve was plotted using the ABT-737 parent ion (813 m/z, $[M+H]^+$) signal and the Angiotensin II internal standard signal (1046 m/z, $[M+H]^+$). A limit of detection of 0.3 ng was determined from the standard deviation of the response and the slope of the curve. Using the calibration equation, a typical mass of drug per middle-MCS slice was estimated to be 0.81 ng, 1.22 ng, 1.41 ng, 1.75 ng, and 2.47 ng for the 10 µM, 15 µM, 25 µM, 50 µM and 100 µM ABT-737 concentration in the cell culture media over 24h, respectively. Signals for MCCs treated below 5 µM for 24h (slightly above our LOD) were not observed. Extrapolating these numbers based on the area of the drug relative to the slice and the MCS volume, 474 ng, 719 ng, 831 ng, 1031 ng, and 1457 ng for the 10 µM, 15 µM, 25 µM, 50 µM and 100 µM during 24h incubation, respectively are estimated per MCS. This methodology allows for further assessment of the ABT-737 generated toxicity at the MCS level. This method is particularly advantageous for cases when the drug is localized and is not homogenously distributed across the MCS or cancer tumor.

Conclusions

An analytical workflow capable of estimating the amount of drug incorporated per MCS based and their localization based on complementary TOF-SIMS and LESA-TIMS-TOF MS/MS is described. The use of TOF-SIMS allowed for high spatial resolution chemical mapping (~1.2 µm) of ABT-737 drug in single MCS slices. Complementary, *in-situ* LESA-TIMS-TOF MS using internal standards allowed secondary confirmation based on mobility selected fragmentation pattern and 3D quantitation of the amount of ABT-737 drug per MCS slices. This methodology enables further assessment of the fate and uptake of drugs by cancer tumors, particularly when drugs are not homogenously distributed inside the tumor volume.

Acknowledgements

YCD acknowledge the financial support from NSF FGLSAMP FIU Bridge to the Doctorate award HRD # 1810974. AC was fully supported by NSF grant HRD-1547798 awarded to Florida International University as part of the Centers for Research Excellence in Science and Technology (CREST) Program.

References

1. X. Cui, Y. Hartanto and H. Zhang, *J R Soc Interface*, 2017, **14**.
2. L. B. Weiswald, D. Bellet and V. Dangles-Marie, *Neoplasia*, 2015, **17**, 1-15.
3. Y. Fang and R. M. Eglen, *SLAS discovery : advancing life sciences R & D*, 2017, **22**, 456-472.
4. M. Sans, K. Gharpure, R. Tibshirani, J. Zhang, L. Liang, J. Liu, J. H. Young, R. L. Dood, A. K. Sood and L. S. Eberlin, *Cancer Research*, 2017, **77**, 2903-2913.
5. S. Guenther, L. J. Muirhead, A. V. Speller, O. Golf, N. Strittmatter, R. Ramakrishnan, R. D. Goldin, E. Jones, K. Veselkov, J. Nicholson, A. Darzi and Z. Takats, *Cancer Research*, 2015, **75**, 1828-1837.
6. J. F. Timms, O. J. Hale and R. Cramer, *Expert Review of Proteomics*, 2016, **13**, 593-607.
7. M. Sans, C. L. Feider and L. S. Eberlin, *Current opinion in Chemical Biology*, 2018, **42**, 138-146.
8. M. Sun, X. Tian and Z. Yang, *Analytical Chemistry*, 2017, **89**, 9069-9076.
9. H. Li and A. B. Hummon, *Anal Chem*, 2011, **83**, 8794-8801.
10. X. Liu, E. M. Weaver and A. B. Hummon, *Analytical Chemistry*, 2013, **85**, 6295-6302.
11. L. J. Gamble and C. R. Anderton, *Microscopy today*, 2016, **24**, 24-31.
12. Q. P. Vanbellingen, A. Castellanos, M. Rodriguez-Silva, I. Paudel, J. W. Chambers and F. A. Fernandez-Lima, *Journal of the American Society for Mass Spectrometry*, 2016, **27**, 2033-2040.
13. S. Ninomiya, K. Yoshimura, L. C. Chen, S. Takeda and K. Hiraoka, *Mass Spectrometry*, 2017, **6**, A0053.
14. J. R. N. Haler, E. K. Sisley, Y. L. Cintron-Diaz, S. N. Meitei, H. J. Cooper and F. Fernandez-Lima, *Analytical Methods*, 2019, **11**, 2385-2395.
15. S. S. Basu, E. C. Randall, M. S. Regan, B. G. C. Lopez, A. R. Clark, N. D. Schmitt, J. N. Agar, D. A. Dillon and N. Y. R. Agar, *Analytical Chemistry*, 2018, **90**, 4987-4991.
16. V. A. Mikhailov, R. L. Griffiths and H. J. Cooper, *International Journal of Mass Spectrometry*, 2017, **420**, 43-50.
17. D. J. Ryan, D. Nei, B. M. Prentice, K. L. Rose, R. M. Caprioli and J. M. Spraggins, *Rapid Communications in Mass Spectrometry*, 2018, **32**, 442-450.
18. J. Havlikova, E. C. Randall, R. L. Griffiths, J. G. Swales, R. J. A. Goodwin, J. Bunch, I. B. Styles and H. J. Cooper, *Analytical Chemistry*, 2019, DOI: 10.1021/acs.analchem.9b04148.
19. D. J. Ryan, N. H. Patterson, N. E. Putnam, A. D. Wilde, A. Weiss, W. J. Perry, J. E. Cassat, E. P. Skaar, R. M. Caprioli and J. M. Spraggins, *Analytical Chemistry*, 2019, **91**, 7578-7585.
20. H. Borsdorf and G. A. Eiceman, *Applied Spectroscopy Review*, 2006, **41**, 323-375.
21. E. K. Sisley, E. Illes-Toth and H. J. Cooper, *TrAC Trends in Analytical Chemistry*, 2019, DOI: https://doi.org/10.1016/j.trac.2019.05.036.
22. R. L. Griffiths, A. J. Creese, A. M. Race, J. Bunch and H. J. Cooper, *Analytical Chemistry*, 2016, **88**, 6758-6766.
23. D. Eikel, M. Vavrek, S. Smith, C. Bason, S. Yeh, W. A. Korfmacher and J. D. Henion, *Rapid communications in mass spectrometry*, 2011, **25**, 3587-3596.
24. W. B. Parson, S. L. Koeniger, R. W. Johnson, J. Erickson, Y. Tian, C. Stedman, A. Schwartz, E. Tarcsa, R. Cole and G. J. Van Berkel, *Journal of Mass Spectrometry*, 2012, **47**, 1420-1428.
25. E. E. G. Rebekah L Zinn, Irina Dobromilskaya, Sara Murphy, Luigi Marchionni, Christine L Hann and and C. M. Rudin*, *Molecular Cancer*, 2013, **12**.
26. M. Broecker-Preuss, N. Becher-Boveleth, S. Muller and K. Mann, *Cancer cell international*, 2016, **16**, 27.
27. R. D. McCulloch and M. Amo-Gonzalez, *Rapid communications in mass spectrometry*, 2019, **33**, 1455-1463.
28. H. Chen, C. Chen, W. Huang, M. Li, Y. Xiao, D. Jiang and H. Li, *Analytical Chemistry*, 2019, **91**, 9138-9146.
29. J. Le Maitre, M. Hubert-Roux, B. Paupy, S. Marceau, C. P. Ruger, C. Afonso and P. Giusti, *Faraday discussions*, 2019, **218**, 417-430.
30. E. A. Rue, J. A. Glinski, V. B. Glinski and R. B. van Breemen, *Journal of Mass Spectrometry*, 2019, DOI: 10.1002/jms.4377.
31. F. A. Fernandez-Lima, D. A. Kaplan and M. A. Park, *Review of Scientific Instruments*, 2011, **82**, 126106.
32. F. Fernandez-Lima, D. Kaplan, J. Suetering and M. Park, *International Journal for Ion Mobility Spectrometry*, 2011, **14**, 93-98.
33. K. Jeanne Dit Fouque and F. Fernandez-Lima, *TrAC Trends in Analytical Chemistry*, 2019, **116**, 308-315.
34. K. J. Adams, D. Montero, D. Aga and F. Fernandez-Lima, *International Journal for Ion Mobility Spectrometry*, 2016, **19**, 69-76.
35. A. McKenzie-Coe, J. D. DeBord, M. Ridgeway, M. Park, G. Eiceman and F. Fernandez-Lima, *The Analyst*, 2015, **140**, 5692-5699.
36. P. Benigni, R. Marin and F. Fernandez-Lima, *International Journal for Ion Mobility Spectrometry*, 2015, **18**, 151-157.
37. K. J. Adams, C. E. Ramirez, N. F. Smith, A. C. Munoz-Munoz, L. Andrade and F. Fernandez-Lima, *Talanta*, 2018, **183**, 177-183.
38. K. J. Adams, N. F. Smith, C. E. Ramirez and F. Fernandez-Lima, *International Journal of Mass Spectrometry*, 2018, **427**, 133-140.
39. A. Garabedian, M. A. Baird, J. Porter, K. Jeanne Dit Fouque, P. V. Shliaha, O. N. Jensen, T. D. Williams, F. Fernandez-Lima and A. A. Shvartsburg, *Analytical Chemistry*, 2018, **90**, 2918-2925.
40. F. Meier, A. D. Brunner, S. Koch, H. Koch, M. Lubeck, M. Krause, N. Goedecke, J. Decker, T. Kosinski, M. A. Park, N. Bache, O. Hoerning, J. Cox, O. Rather and M. Mann, *Molecular & cellular proteomics*, 2018, **17**, 2534-2545.
41. K. Jeanne Dit Fouque, C. E. Ramirez, R. L. Lewis, J. P. Koelmel, T. J. Garrett, R. A. Yost and F. Fernandez-Lima, *Analytical Chemistry*, 2019, **91**, 5021-5027.
42. A. Garabedian, D. Butcher, J. L. Lippens, J. Miksovska, P. P. Chapagain, D. Fabris, M. E. Ridgeway, M. A. Park and F. Fernandez-Lima, *Physical Chemistry Chemical Physics : PCCP*, 2016, **18**, 26691-26702.
43. D. Butcher, P. Chapagain, F. Leng and F. Fernandez-Lima, *The journal of physical chemistry. B*, 2018, **122**, 6855-6861.
44. J. Friedrich, C. Seidel, R. Ebner and L. A. Kunz-Schughart, *Nature protocols*, 2009, **4**, 309-324.

45. W. Senkowski, X. Zhang, M. H. Olofsson, R. Isacson, U. Hoglund, M. Gustafsson, P. Nygren, S. Linder, R. Larsson and M. Fryknas, *Molecular cancer therapeutics*, 2015, **14**, 1504-1516.
46. X. Gong, C. Lin, J. Cheng, J. Su, H. Zhao, T. Liu, X. Wen and P. Zhao, *PloS one*, 2015, **10**, 1-18.
47. K. Okumura, S. Huang and F. A. Sinicrope, *Clinical Cancer Res*, 2008, **14**, 8132-8142.
48. C. Tse, A. R. Shoemaker, J. Adickes, M. G. Anderson, J. Chen, S. Jin, E. F. Johnson, K. C. Marsh, M. J. Mitten, P. Nimmer, L. Roberts, S. K. Tahir, Y. Xiao, X. Yang, H. Zhang, S. Fesik, S. H. Rosenberg and S. W. Elmore, *Cancer Research*, 2008, **68**, 3421-3428.
49. E. W. McDaniel and E. A. Mason, *Mobility and diffusion of ions in gases*, John Wiley and Sons, Inc., New York, New York, 1973.
50. A. Brunelle, D. Touboul and O. Laprevote, *Journal of mass spectrometry*, 2005, **40**, 985-999.
51. J. Hoarau-Vechot, A. Rafii, C. Touboul and J. Pasquier, *International journal of molecular sciences*, 2018, **19**.
52. D. Lv, Z. Hu, L. Lu, H. Lu and X. Xu, *Oncology letters*, 2017, **14**, 6999-7010.
53. F. Hirschhaeuser, H. Menne, C. Dittfeld, J. West, W. Mueller-Klieser and L. A. Kunz-Schughart, *Journal of Biotechnology*, 2010, **148**, 3-15.
54. J. D. DeBord, D. F. Smith, C. R. Anderton, R. M. Heeren, L. Pasa-Tolic, R. H. Gomer and F. A. Fernandez-Lima, *PloS one*, 2014, **9**, e99319.
55. S. Cory and J. M. Adams, *Cancer Cell*, 2005, **8**, 5-6.